ChemPubSoc Europe

DOI: 10.1002/chem.201604162

CHEMISTRY A European Journal Full Paper

Electrocatalysis

Synthesis of Cobalt Sulfide/Sulfur Doped Carbon Nanocomposites with Efficient Catalytic Activity in the Oxygen Evolution Reaction

Huayu Qian,[a] Jing Tang,*[b] Zhongli Wang,[b] Jeonghun Kim,[c] Jung Ho Kim,[c] Saad M. Alshehri,[d] Ekrem Yanmaz,[e] Xin Wang,*[a] and Yusuke Yamauchi*[b, c]

Abstract: Cobalt sulfide/sulfur doped carbon composites (Co_9S_8/S-C) were synthesized by calcining a rationally designed sulfur-containing cobalt coordination complex in an inert atmosphere. From the detailed transmission electron microscopy (TEM) and X-ray photoelectron spectroscopy (XPS) analyses, the electrocatalytically active Co_9S_8 nanoparticles were clearly obtained and combined with the thin sulfur doped carbon layers. Electrochemical data showed that Co_9S_8/S-C had a good activity and long-term stability in catalyzing oxygen evolution reaction in alkaline electrolyte, even better than the traditional RuO_2 electrocatalyst. The excellent electrocatalytic activity of Co_9S_8/S-C was mainly attributed to the synergistic effect between the Co_9S_8 catalyst which contributed to the oxygen evolution reaction and the sulfur doped carbon layer which facilitated the adsorption of reactants, prevented the Co_9S_8 particles from aggregating and served as the electrically conductive binder between each component.

Introduction

The hydrogen economy is one of the most promising solutions to deal with the up-coming depletion of fossil fuels and the ever-worsening environmental problems in modern society.[1] This system relies on large-scale hydrogen source supplied by clean and sustainable techniques, such as electrochemically water splitting.[2] The anode reaction, namely oxygen evolution reaction (OER, $4OH^- \rightarrow 2H_2O + O_2 + 4e^-$, in alkaline solution) is one of the main steps in electrochemically water splitting.[3] However, sluggish reaction kinetics of the OER still limits the whole water splitting reaction.[4] Therefore, high efficiency electrocatalysts are required to further accelerate the reaction. Despite the traditional ruthenium- or iridium-based electrocatalysts are among the most active OER electrocatalysts, the prohibitive cost and inevitable dissolution[5] prevent their large-scale application in electrochemically water splitting.

To date, tremendous efforts have been devoted to develop cost-effective and durable electrocatalysts. Recent studies found that some of the first row transition metal sulfides (for example, CoS, Co_9S_8,[6] Ni_3S_2[7]) have good electrocatalytic activity. Among them, the Co_9S_8 has been demonstrated as a high-performance catalyst for both the oxygen reduction reaction (ORR)[8] and hydrogen evolution reaction (HER).[9] However, the quantitative OER performance of Co_9S_8 is still insufficient.[10] Many innovative methods have been applied to improve the OER activity of Co_9S_8. One method is to combine Co_9S_8 with other OER active catalysts. For example, Zhu et al. designed the Co_9S_8@MoS_2 core–shell catalyst, and achieved enhanced HER and OER activities compared with the single Co_9S_8 catalyst.[11] Wang et al. used Ni to promote the OER and HER activity of cobalt sulfide.[12] Another effective method is to combine Co_9S_8 with porous and electron conductive materials, which can not only enhance the electron transference, but also protect the Co_9S_8 particles from aggregating.[13]

Nanostructured carbons are known to have unique characteristics such as high electron conductivity, high chemical stability and high surface area.[14] Based on this background, Ganesan et al. designed an OER active electrocatalyst of nitrogen and sulfur co-doped graphene oxide supported cobalt sulfide by thermal treating of cobalt thiourea complex/graphene oxide mixture.[15] Liu et al. prepared a Co_3S_4@N/S-rGO composite using solvothermal reaction.[16] However, multiple synthetic steps are usually required in the previous reports. In recent years, metal–organic frameworks (MOFs) have become a fascinating self-templated precursors for preparing diverse nano-

[a] H. Qian, Prof. X. Wang
Key Laboratory for Soft Chemistry and Functional Materials of Ministry Education, Nanjing University of Science and Technology
210094, Nanjing (P. R. China)
E-mail: wangx@njust.edu.cn

[b] Dr. J. Tang, Dr. Z. Wang, Prof. Y. Yamauchi
International Center for Materials Nanoarchitectonics (MANA)
National Institute for Materials Science (NIMS)
1–1 Namiki, Tsukuba, Ibaraki 305-0044 (Japan)
E-mail: tang.Jing@nims.go.jp
yamauchi.yusuke@nims.go.jp

[c] Dr. J. Kim, Prof. J. H. Kim, Prof. Y. Yamauchi
Australian Institute for Innovative Materials (AIIM)
University of Wollongong, North Wollongong, NSW 2500 (Australia)

[d] Prof. S. M. Alshehri
Department of Chemistry, College of Science
King Saud University, Riyadh 11451 (Saudi Arabia)

[e] Prof. E. Yanmaz
Department of Mechatronics, Faculty of Engineering and Architecture
Gelisim University, Istanbul 34315 (Turkey)

Supporting information for this article is available on the WWW under http://dx.doi.org/10.1002/chem.201604162.

materials with regular porous morphologies, including carbon-based materials,[17] metal oxides,[18] metal phosphides,[19] and metal sulfides,[20] because of the diverse structures formed with high surface area, controlled pore volume,[21,22] interconnected pores,[23] and the alterable organic linker and metal ion pairs in the MOFs. Herein, we present a simple method to synthesize a cobalt sulfide/sulfur doped carbon composite by one-step calcination of a designed metal–organic coordination complex that consists of cobalt ions and sulfur-rich organic linkers. The synthetic processes are illustrated in Scheme 1. First, 2-methylimidazole (MeIm) and 4-imidazoledithiocarboxylic acid (ImTA) are used as the organic linkers to coordinate together with the subsequently added cobalt ions. After reacting for 12 h, the cobalt-MeIm-ImTA coordination complex is precipitated and collected. Then, the coordination complex was simply calcined under an inert atmosphere. During the calcination process, the MeIm and ImTA decompose at high temperature. Some of the sulfur atoms from the ImTA react with cobalt ions and form cobalt sulfide. Furthermore, some of the sulfur atoms were retained in porous carbon matrix. Finally, the cobalt sulfide/sulfur doped carbon composite was formed and was studied as the catalyst for OER.

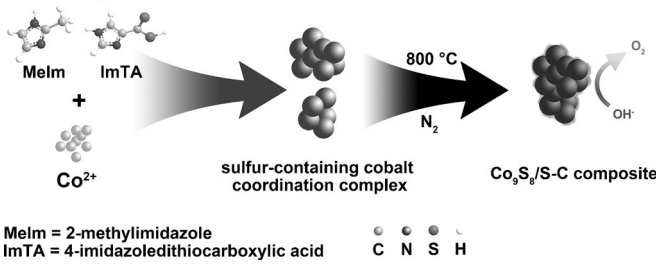

Scheme 1. Illustration of the synthesis of cobalt sulfide/sulfur doped carbon composite (Co_9S_8/S-C) from a sulfur-containing cobalt coordination complex.

Results and Discussion

Characterization of cobalt sulfide/sulfur doped carbon composite

The XRD patterns of cobalt sulfide/sulfur doped carbon composites (Co_9S_8/S-C-*x*) obtained at different temperatures (600 °C, 700 °C, and 800 °C) are presented in Figure 1a. All of the three composites displayed obvious diffraction peaks that corresponded well to the Co_9S_8 XRD patterns (JCPDS card no. 65-6801). Comparing the three patterns of Co_9S_8/S-C-*x*, we found that the peak intensity of Co_9S_8 was higher with increased calcination temperatures, indicating the higher crystallinity and larger particle sizes of Co_9S_8 in the composite. Moreover, by further examining the high-resolution XRD patterns at 2θ of 44.0° to 45.0° with a scan rate of 0.1° min^{-1}, a weak diffraction peak at 44.2° is found in Co_9S_8/S-C-700 and Co_9S_8/S-C-800, which can be attributed to the metallic Co (111) facet reflection (JCPDS card no. 15-0806). The traceable metallic cobalt was formed due to the carbothermic reduction of a small amount of cobalt ions at relative high temperature above 700 °C in N_2 gas. On the other hand, no noticeable carbon diffraction peaks were shown in XRD patterns because of the low content and low crystallinity of carbon component in Co_9S_8/S-C-*x*.

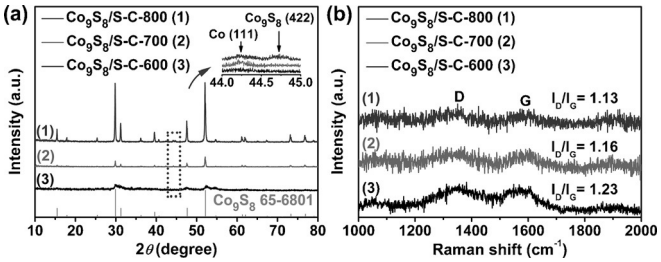

Figure 1. a) XRD patterns and b) Raman spectra of Co_9S_8/S-C-600, Co_9S_8/S-C-700 and Co_9S_8/S-C-800.

Raman spectra of the synthesized Co_9S_8/S-C-*x* composite were evaluated to study the carbon component, which is not observed in the XRD measurement. From Figure 1b, all of the three Co_9S_8/S-C-*x* composites displayed the peaks located at about 1344 cm^{-1} and 1583 cm^{-1}, which are the typical D and G bands of carbon materials,[24] indicating that carbon was retained after calcining the Co-MeIm-ImTA coordination complex. Meanwhile, the intensity ratios of D band and G band (I_D/I_G) in each of Co_9S_8/S-C-*x* composite decreased with increasing temperature, revealing the increased graphitization degree of carbon in Co_9S_8 composite.[25]

XPS data can help to obtain detailed information of the superficial elements. Figure 2a exhibits the survey scan showing that main elements in Co_9S_8/S-C-800 are carbon, oxygen, a small amount of sulfur, and cobalt. The atomic content of

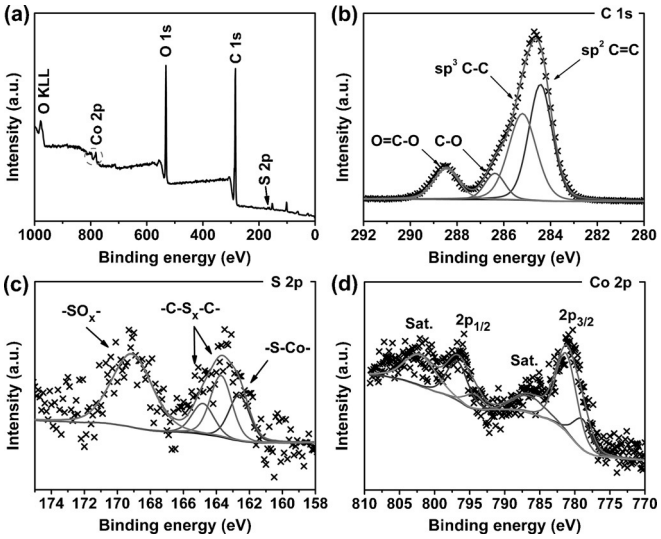

Figure 2. a) XPS survey spectrum of Co_9S_8/S-C-800; b)–d) high-resolution C 1s (b), S 2p (c), and Co 2p (d) spectra of Co_9S_8/S-C-800.

each element was C 70.1, O 28.2, S 0.7, and Co 0.5%. Such high C and O ratios calculated from XPS data of Co_9S_8/S-C-800 was attributed to the unique structure of Co_9S_8/S-C-800 in which Co_9S_8 particles were separated by carbon layers that have plenty of oxygen-containing functional groups. The carbon layers partially sheltered the photoelectrons from the inner Co_9S_8 structure in XPS measurement. From a high-resolution XPS scan of C 1s in Figure 2b, the C 1s peak was deconvoluted into four constituents, including graphitic carbon (sp^2 C=C, ca. 284.5 eV), amorphous carbon (mainly sp^3 C–C, ca. 285.3 eV), phenolic or alcoholic carbon (C–O, ca. 286.4 eV), and carboxyl (O–C=O, ca. 288.4 eV).[26] The C–S peak in the C 1s spectrum is weak and appears at 283.9 eV,[27] which overlaps with the main graphitic carbon peak. As a result, the C–S peak was not indicated in the C 1s spectrum. The detailed information of sulfur could be investigated from the deconvoluted high resolution S 2p spectrum in Figure 2c. The broad peak at lower binding energy consisted of three peaks. The peaks at 163.7 eV and 164.8 eV were the S $2p_{3/2}$ and S $2p_{1/2}$ state, which correspond to a –C–S_x–C– structure,[28] indicating sulfur atoms doped in carbon. The other peak with a binding energy of 162.6 eV was attributed to the sulfur in cobalt sulfide.[29] Another peak at higher binding energy (169.1 eV) was the oxidized sulfur from –SO_x–.[30,31] The Co 2p spectrum in Figure 2d consists of a doublet corresponding to Co $2p_{3/2}$ and Co $2p_{1/2}$ orbital splitting. In the range of Co $2p_{3/2}$, the peaks at 778.9 eV and ca. 781.2 eV with the shakeup at about 786.5 eV were attributed to cobalt species in Co_9S_8 mixed with cobalt oxide, which came from surface oxidation of metallic Co.[11,32]

The overall morphology of the as synthesized Co-MeIm-ImTA and Co_9S_8/S-C-*x* was observed by SEM. From Figure 3a, the Co-MeIm-ImTA coordination complex was mainly composed of irregular nanoparticles with an average particle size of about 50 nm. The Co_9S_8/S-C particles remained discrete and separated when Co-MeIm-ImTA was calcined at 600 °C (Figure 3b). However, with increasing calcination temperature, the Co_9S_8 particles in Co_9S_8/S-C-700 and Co_9S_8/S-C-800 aggregated with other Co_9S_8 particles, forming a smooth surface (Figure 3c,d). The detailed particle size distribution histograms of each sample calculated from SEM images are shown in the Supporting Information, Figure S1.

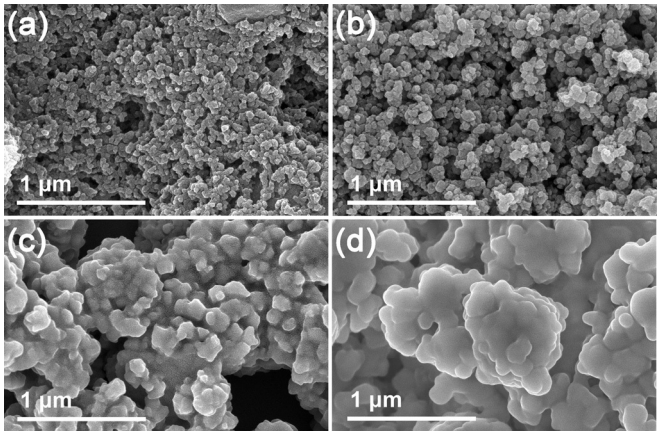

Figure 3. SEM images of a) Co-MeIm-ImTA, b) Co_9S_8/S-C-600, c) Co_9S_8/S-C-700, and d) Co_9S_8/S-C-800.

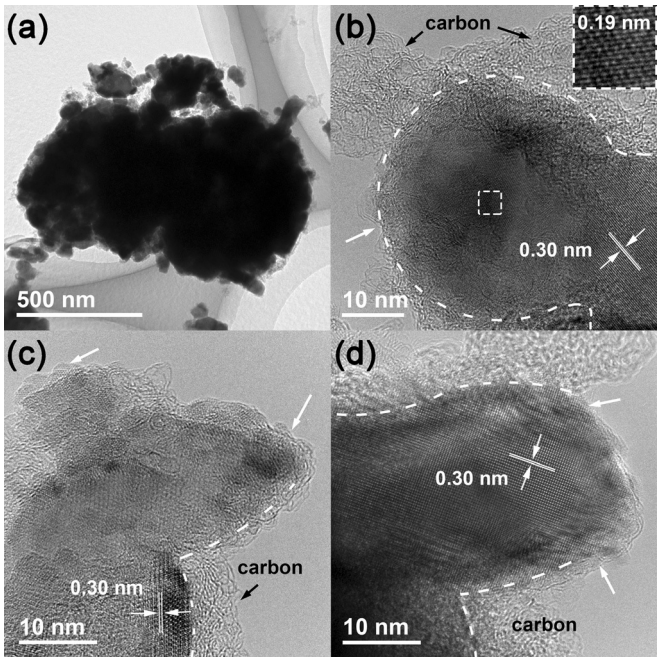

Figure 4. a) TEM image of Co_9S_8/S-C-800; b)–d) high-resolution TEM images of Co_9S_8/S-C-800. White arrows indicate exposed spots of Co_9S_8 particle.

The detailed morphology of Co_9S_8/S-C-800 particles was investigated by TEM. As shown in Figure 4a, an aggregated large particle of Co_9S_8/S-C-800 was composed of smaller particles adherent to each other. The high-resolution TEM (HRTEM) image of Co_9S_8/S-C-800 is shown in Figure 4b–d. Lattice fringes with a *d*-spacing of 0.19 nm (inset in Figure 4b) and 0.30 nm (Figure 4b–d) were observed inside the particle, corresponding to the (511) and (311) crystal planes of Co_9S_8, respectively. Besides, carbon layers 2–10 nm thick were found partially covering the Co_9S_8 particles (Figure 4b–d). The carbon component played two important roles in the composite, not only protecting the Co_9S_8 particles from serious aggregating but also serving as conductive bridges between Co_9S_8 particles and the electrode. Furthermore, the element distribution of Co_9S_8/S-C-800 was investigated by elemental mapping. As seen in Figure 5, the Co_9S_8/S-C-800 composite consisted of the 4 main elements C, O, S, and Co. The EDX spectrum of Co_9S_8/S-C-800 is shown in the Supporting Information, Figure S2, which shows that the carbon layers bonded the cores that mainly composed of Co and S, indicating the fine combination between carbon and Co_9S_8 in Co_9S_8/S-C-800.

For better understanding, a wide-angle XRD pattern, EDX spectrum, TEM images, element distribution information, and TGA data for Co-MeIm-ImTA coordination complex were obtained (Supporting Information, Figures S3–S5). Wide-angle XRD shows no diffraction peaks, indicating an amorphous state of Co-MeIm-ImTA complex as shown in the Supporting Information, Figure S3. In sharp contrast to MeIm, two S atoms in the ImTA molecules exhibit stronger interaction to Co^{2+} ions

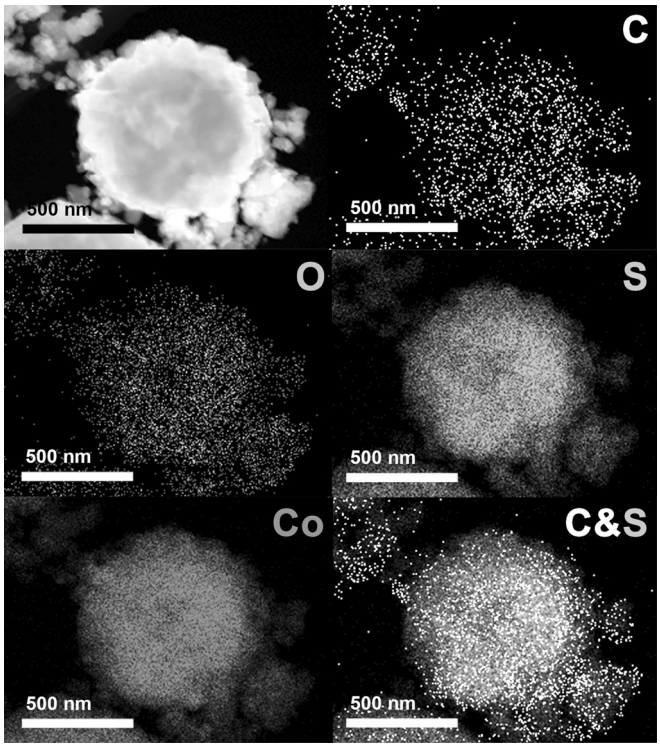

Figure 5. HAADF-STEM image, and elemental mappings of one large particle of Co_9S_8/S-C-800.

compared to two N atoms in the imidazole ring. The coordination bonding between the Co^{2+} ions and two N atoms in the imidazole ring is critical for formation of the ordered long-term crystal structure (for example, ZIF-67 consisting of Co-MeIm).[33] In the present study, adding 5 mol% of ImTA molecules probably interrupted the crystalline formation, resulting in a disordered structure. The elemental mapping images (Supporting Information, Figure S4) revealed that the C, N, S, and Co atoms are well distributed at the same area, indicating the uniform composition of the sulfur-containing cobalt coordination complex. As seen in the Supporting Information, Figure S5, when the calcining temperature was below 300 °C, the main structure of Co-MeIm-ImTA coordination complex was stable while the weight loss was caused by solvent evaporation. The complex encountered thermal decomposition when the temperature increased from 300 °C to 500 °C, resulting in the fast weight loss. During this process, the active sulfur element can react with cobalt ions (Co^{2+}) and form Co_9S_8 small grains. The organic linkers of MeIm and ImTA would be converted into sulfur doped porous carbon and distributed between the Co_9S_8 grains. When the temperature increased above 700 °C, small Co_9S_8 grains grew to be larger nanoparticles, as shown in SEM images (Figure 3) and the particle size distribution histograms (Supporting Information, Figure S1). The weight loss occurring at around 750 °C was probably due to the further decomposition of the unstable sulfur-doped carbons as well as the oxygen functional groups at high temperature.[34,35] Finally, the yield of carbonization was 34% according a TG curve (Supporting Information, Figure S5).

OER performance of the cobalt sulfide/sulfur doped carbon composite

The OER catalytic performance of the Co_9S_8/S-C-*x* composite and RuO_2 was evaluated by LSV in 1 M KOH solution performed at 1.2 to 1.7 V vs. RHE. From the LSV curves shown in Figure 6a, Co_9S_8/S-C-800 exhibited the lowest onset potential at

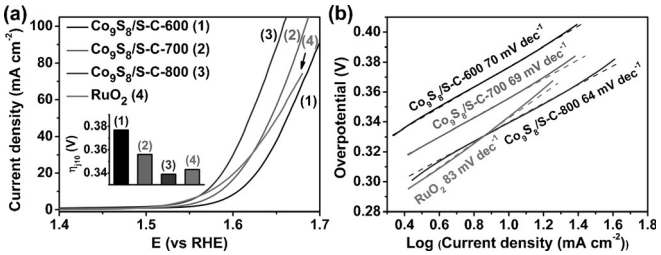

Figure 6. a) LSV curves of Co_9S_8/S-C-600, Co_9S_8/S-C-700, Co_9S_8/S-C-800, and RuO_2 with 95% *iR* compensation; b) the corresponding Tafel slopes of Co_9S_8/S-C-600, Co_9S_8/S-C-700, Co_9S_8/S-C-800, and RuO_2.

about 1.51 V, which is similar to the traditional RuO_2 catalyst (ca. 1.50 V). The onset potential of all of the catalysts followed the reverse order of calcination temperature: Co_9S_8/S-C-800 ≈ RuO_2 < Co_9S_8/S-C-700 < Co_9S_8/S-C-600, indicating lower energy barrier in OER process on Co_9S_8/S-C-800. The overpotential at the current density reach of 10 mA cm^{-2} (denoted as η_{j10}) is usually used to evaluate the OER catalysts. The inset of Figure 6a provides the η_{j10} of each catalyst. It can be seen that Co_9S_8/S-C-800 exhibits the lowest overpotential (0.339 V) among the three Co_9S_8/S-C samples, which is even lower to commercial RuO_2 (ca. 0.343 V). This result demonstrates the high OER activity of the Co_9S_8/S-C-800 catalyst. Tafel plots calculated from LSV data are a much more straightforward way to estimate the OER kinetics of the catalysts. Figure 6b shows that the Tafel slope of Co_9S_8/S-C-800 was 64 mV per decade, which is smaller than commercial RuO_2 catalyst (83 mV per decade) and is close to the other two Co_9S_8/S-C catalysts. The small Tafel slope suggested that the Co_9S_8/S-C-800 has higher OER kinetics efficiency than RuO_2. Moreover, as indicated from the similar Tafel slops of the three Co_9S_8/S-C-*x* composites, these Co_9S_8/S-C-*x* OER catalysts had the same reaction mechanism in the water oxidation reaction.[10,36,37] Additionally, the long-term electrocatalytic stability of Co_9S_8/S-C-800 was tested by continuous CV scan and the results are shown in the Supporting Information, Figure S6. The Co_9S_8/S-C-800 has better stability than RuO_2 catalyst during the 1000 cycle CV tests.

The enhanced OER activity of cobalt sulfide/sulfur doped carbon composite can be attributed to the cooperative effects from individual components: 1) The exposed spots on the Co_9S_8 surfaces provided fundamental OER activity in alkaline media, and the carbon layer between Co_9S_8 particles served as the conductive binder and separator for nanosized Co_9S_8 particles; 2) the heteroatoms in carbon also played an important role in OER process; the sulfur atom has larger atomic radius than carbon, and the lone pairs of sulfur could facilitate the in-

teraction with the molecules in the electrolyte;[38] and 3) the small amount of metallic cobalt which exists in the Co_9S_8/S-C composite also increases the conductivity of Co_9S_8/S-C composite.

Conclusion

A sulfur-containing cobalt coordination complex was synthesized by using 4-imidazoledithiocarboxylic acid, which contains sulfur as the carbon precursor. The complex was subsequently converted into cobalt sulfide/sulfur doped carbon composite by a high-temperature calcination process. The resulting Co_9S_8/S-C-800 catalyst exhibits high performance for OER in alkaline electrolyte. The high OER activity and durability were mainly attributed to the synergistic effect among the individual components of Co_9S_8, metallic Co, and the heteroatom-doped carbon layer. This provides a design for directly converting metal–organic coordination complexes into a metal sulfide/carbon composite structure, and it can be extended to design other innovative composites with unique structure by simple synthetic procedures.

Experimental Section

Materials: Cobalt nitride hexahydrate ($Co(NO_3)_2{\cdot}6H_2O$, 99.5%) and ruthenium dioxide (RuO_2) were purchased from Wako Pure Chemical Industries, Ltd. 2-methylimidazole (98%), dimethylformamide (DMF), and methanol (MeOH) were obtained from Nacalai Tesque Reagent Co. 4-imidazoledithiocarboxylic acid (70%, technical grade) and 5% Nafion solution were purchased from Sigma–Aldrich Chemical Co. All solutions were prepared using 18 MΩ ultrapure water from Milli-Q system.

Preparation of sulfur-containing cobalt coordination complex: In a typical synthesis, 4-imidazoledithiocarboxylic acid (ImTA, 72 mg) was washed twice in MeOH (35 mL) and dissolved in DMF (10 mL). Then, 28% ammonia solution (24 μL) was added to the ImTA solution and stirred for 5 min. Subsequently, $Co(NO_3)_2{\cdot}6H_2O$ (534 mg) in MeOH solution (10 mL) and MeIm (546 mg) in MeOH (10 mL) were added successively under vigorously stirring. After stirring for 5 min, the mixture was set aside and aged for 12 h at room temperature. The brown precipitate was collected by 10000 rpm centrifugation, washed with DMF and MeOH, and dried at 60 °C. The resulting sulfur-containing cobalt coordination complex was denoted as Co-MeIm-ImTA.

Synthesis of cobalt sulfide/sulfur doped carbon composite: Cobalt sulfide/sulfur doped carbon composite was obtained by thermal treatment of sulfur-containing cobalt coordination complexes under nitrogen atmosphere. Typically, Co-MeIm-ImTA (100 mg) was placed in an alumina ceramic boat and heated to the target temperatures at a heating rate of 1 °C per minute under the protection of nitrogen gas flow in a tubular furnace, then kept at the target temperature for 3 h and cooled down to room temperature. The products were labelled as Co_9S_8/S-C-*x*, where *x* refers the target calcination temperature of 600, 700, or 800 °C.

Characterization: Powder X-ray diffraction (XRD) patterns were obtained on an Ultima Rint 2000 X-ray diffractometer (RIGAKU, Japan) using Cu Kα radiation (40 kV, 40 mA, 2° min^{-1} scan rate). Raman spectra were recorded on a Horiba-Jovin Yvon T64000 operating with 514 nm laser source. X-ray photoelectron spectroscopy (XPS) spectra were measured by a Japanese PHI Quantera II system (ULVAC-PHI) using Al Kα X-ray radiation ($E = 1486.6$ eV) operated at room temperature. Thermal properties of the precursors were tested by thermogravimetry analysis (TGA) on a Hitachi HT-Seiko Instrument Exter 6300 TG/DTA system. Each sample was heated from room temperature to 800 °C in a platinum pot with a heating rate of 5 °C min^{-1} under nitrogen gas protection. The overall morphology of the samples was characterized on a Hitachi SU8000 field emission scanning electron microscope (FESEM) operating at 5 kV. Before SEM observation, platinum coating was applied to ensure clear SEM images. Specific morphology, high angle annular dark field scanning transmission electron microscopy (HAADF-STEM) images, and element analysis mapping were obtained on a JEOL JEM-2100F field emission transmission electron microscope (FETEM).

Electrochemical measurements: All electrochemical experiments were conducted on a CHI 660EZ (CH Instruments, USA) electrochemistry workstation using a three-electrode cell. In the cell, a 3 mm (0.0707 cm^2) diameter glassy carbon (GC) electrode coated with sample was placed horizontally in the electrolyte and served as the working electrode. A 6 mm diameter graphite rod was placed as the counter electrode opposite to the working electrode, and a double salt bridge isolated Ag/AgCl electrode (3 M NaCl, 0.195 V vs. RHE) was used as the reference electrode. The ink was prepared by dispersing 2 mg of one sample in 1 mL solution (water/ethanol/5% Nafion solution = 15:5:1 volume ratio) by ultrasonication. Before applying the ink, GC electrodes were polished by 1 μm diamond and 0.05 μm alumina powder respectively, rinsed with sufficient water and dried under nitrogen gas flow. Then 9 μL ink was dropped on the GC electrode to form 0.25 mg cm^{-2} catalyst loading and dried under nitrogen gas flow. The OER activity of the samples was measured in 1 M KOH solution and all of the potentials were converted to RHE based on the formula $E_{RHE} = E_{Ag/AgCl} + 0.195 + 0.059\,pH$.[39] Cyclic voltammograms (CVs) was firstly performed at a scan rate of 10 mV s^{-1} within the potential range of 1.2 to 1.7 V (vs. RHE) for 20 cycles to ensure the electrode reached a stable state. Linear sweep voltammetry (LSV) conducted with the condition of 10 mV s^{-1}, 1.2 to 1.7 V (vs. RHE), 95% *iR* compensation, was repeated 5 times to evaluate the OER activity. Tafel slopes were calculated from LSV polarization curves by plotting overpotential ($\eta = E - E_{O_2}$, $E_{O_2} = 1.229$ V vs. RHE)[40] against log (current density). Stability tests were conducted by continuous CV scan in 1 M KOH solution with a scan rate of 50 mV s^{-1} in the potential window of 1.2–1.7 V (vs. RHE).

Acknowledgements

We acknowledge the financial supported from NSF (No. 51572125) of China and Graduate School of Nanjing University of Science and Technology. The authors also extend their appreciation to the International Scientific Partnership Program (ISPP) at King Saud University (KSU) for funding this research work through ISPP-0024.

Keywords: cobalt sulfide · coordination complex · oxygen evolution reaction · sulfur doped carbon

[1] G. W. Crabtree, M. S. Dresselhaus, M. V. Buchanan, *Phys. Today* **2004**, *57*, 39–44.
[2] M. D. Symes, L. Cronin, *Nat. Chem.* **2013**, *5*, 403–409.
[3] S. Chen, J. J. Duan, M, Jaroniec, S. Z. Qiao, *Adv. Mater.* **2014**, *26*, 2925–2930.

[4] L. Trotochaud, S. L. Young, J. K. Ranney, S. W. Boettcher, *J. Am. Chem. Soc.* **2014**, *136*, 6744 – 6753.
[5] S. Cherevko, S. Geiger, O. Kasian, N. Kulyk, J. P. Grote, A. Savan, B. R. Shrestha, S. Merzlikin, B. Breitbach, A. Ludwig, K. J. J. Mayrhofer, *Catal. Today* **2016**, *262*, 170 – 180.
[6] Z. F. Huang, J. J. Song, K. Li, M. Tahir, Y. T. Wang, L. Pan, L. Wang, X. W. Zhang, J. J. Zou, *J. Am. Chem. Soc.* **2016**, *138*, 1359 – 1365.
[7] G. F. Chen, T. Y. Ma, Z. Q. Liu, N. Li, Y. Z. Su, K. Davey, S. Z. Qiao, *Adv. Funct. Mater.* **2016**, *26*, 3314 – 3323.
[8] J. M. Falkowski, Y. Surendranath, *ACS Catal.* **2015**, *5*, 3411 – 3416.
[9] L. L. Feng, G. D. Li, Y. P. Liu, Y. Y. Wu, H. Chen, Y. Wang, Y. C. Zou, D. J. Wang, X. X. Zou, *ACS Appl. Mater. Interfaces* **2015**, *7*, 980 – 988.
[10] J. Yang, G. X. Zhu, Y. J. Liu, J. X. Xia, Z. Y. Ji, X. P. Shen, S. K. Wu, *Adv. Funct. Mater.* **2016**, *26*, 4712 – 4721.
[11] H. Zhu, J. F. Zhang, R. P. Yanzhang, M. L. Du, Q. F. Wang, G. H. Gao, J. D. Wu, G. M. Wu, M. Zhang, B. Liu, J. M. Yao, X. W. Zhang, *Adv. Mater.* **2015**, *27*, 4752 – 4759.
[12] W. Z. Fang, D. N. Liu, Q. Lu, X. P. Sun, A. M. Asiri, *Electrochem. Commun.* **2016**, *63*, 60 – 64.
[13] B. L. Chen, R. Li, G. P. Ma, X. L. Gou, Y. Q. Zhu, Y. D. Xia, *Nanoscale* **2015**, *7*, 20674 – 20684.
[14] H. Jiang, P. S. Lee, C. Z. Li, *Energy Environ. Sci.* **2013**, *6*, 41 – 53.
[15] P. Ganesan, M. Prabu, J. Sanetuntikul, S. Shanmugam, *ACS catal.* **2015**, *5*, 3625 – 3637.
[16] Q. Liu, J. T. Jin, J. Y. Yan, *ACS Appl. Mater. Interfaces* **2013**, *5*, 5002 – 5008.
[17] J. Tang, R. R. Salunkhe, J. Liu, N. L. Torad, M. Imura, S. Furukawa, Y. Yamauchi, *J. Am. Chem. Soc.* **2015**, *137*, 1572 – 1580.
[18] T. Wang, L. Shi, J. Tang, V. Malgras, S. Asahina, G. G. Liu, H. B. Zhang, X. G. Meng, K. Chang, J. P. He, O. Terasaki, Y. Yamauchi, J. H. Ye, *Nanoscale* **2016**, *8*, 6712 – 6720.
[19] X. Y. Yu, Y. Feng, B. Y. Guan, X. W. (David) Lou, U. Paik, *Energy Environ. Sci.* **2016**, *9*, 1246 – 1250.
[20] R. B. Wu, D. P. Wang, X. H. Rui, B. Liu, K. Zhou, A. W. K. Law, Q. Y. Yan, J. Wei, Z. Chen, *Adv. Mater.* **2015**, *27*, 3038 – 3044.
[21] V. Malgras, Q. M. Ji, Y. Kamachi, T. Z. Mori, F. K. Shieh, K. C.-W. Wu, K. Ariga, Y. Yamauchi, *Bull. Chem. Soc. Jpn.* **2015**, *88*, 1171 – 1200.
[22] K. Ariga, Y. Yamauchi, G. Rydzek, Q. M. Ji, Y. Yonamine, K. C.-W. Wu, J. P. Hill, *Chem. Lett.* **2014**, *43*, 36 – 68.
[23] R. R. Salunkhe, J. Tang, Y. Kamachi, T. Nakato, J. H. Kim, Y. Yamauchi, *ACS nano* **2015**, *9*, 6288 – 6296.
[24] C. Portet, G. Yushin, Y. Gogotsi, *Carbon* **2007**, *45*, 2511 – 2518.
[25] Z. H. Li, M. F. Shao, L. Zhou, R. K. Zhang, C. Zhang, M. Wei, D. G. Evans, X. Duan, *Adv. Mater.* **2016**, *28*, 2337 – 2344.
[26] S. Y. Huang, G. P. Wu, C. M. Chen, Y. Yang, S. C. Zhang, C. X. Lu, *Carbon* **2013**, *51*, 605 – 620.
[27] A. M. El-Sawy, I. M. Mosa, D. Su, C. J. Guild, S. Khalid, R. Joesten, J. F. Rusling, S. L. Suib, *Adv. Energy Mater.* **2016**, *6*, 1501966.
[28] W. Li, M. Zhou, H. M. Li, K. L. Wang, S. J. Cheng, K. Jiang, *Energy Environ. Sci.* **2015**, *8*, 2916 – 2921.
[29] J. Xu, Q. F. Wang, X. W. Wang, Q. Y. Xiang, B. Liang, D. Chen, G. Z. Shen, *ACS nano* **2013**, *7*, 5453 – 5462.
[30] K. Aup-Ngoen, T. Thongtem, S. Thongtem, A. Phuruangrat, *Mater. Lett.* **2013**, *101*, 9 – 12.
[31] C. Zhang, B. An, L. Yang, B. B. Wu, W. Shi, Y. C. Wang, L. S. Long, C. Wang, W. B. Lin, *J. Mater. Chem. A* **2016**, *4*, 4457 – 4463.
[32] Y. J. Sun, C. Liu, D. C. Grauer, J. Yano, J. R. Long, P. D. Yang, C. J. Chang, *J. Am. Chem. Soc.* **2013**, *135*, 17699 – 17702.
[33] X. H. Feng, M. A. Carreon, *J. Cryst. Growth* **2015**, *418*, 158 – 162.
[34] W. Kiciński, A. Dziura, *Carbon* **2014**, *75*, 56 – 67.
[35] L. J. Zhang, Z. X. Su, F. L. Jiang, L. L. Yang, J. J. Qian, Y. F. Zhou, W. M. Li, M. C. Hong, *Nanoscale* **2014**, *6*, 6590 – 6602.
[36] M. S. Burke, M. G. Kast, L. Trotochaud, A. M. Smith, S. W. Boettcher, *J. Am. Chem. Soc.* **2015**, *137*, 3638 – 3648.
[37] W. W. Xu, Z. Y. Lu, X. D. Lei, Y. P. Li, X. M. Sun, *Phys. Chem. Chem. Phys.* **2014**, *16*, 20402 – 20405.
[38] S. A. Wohlgemuth, R. J. White, M. G. Willinger, M. M. Titirici, M. Antonietti, *Green Chem.* **2012**, *14*, 1515 – 1523.
[39] X. Y. Lu, C. Zhao, *Nat. Commun.* **2015**, *6*, 6616.
[40] T. Zhang, C. Wang, S. B. Liu, J. L. Wang, W. B. Lin, *J. Am. Chem. Soc.* **2014**, *136*, 273 – 281.

Received: September 2, 2016
Published online on October 31, 2016